# Virtual Drive Testing of Adaptive Antenna Systems in Dynamic Propagation Scenarios for Vehicle Communications

Fan, Wei; Hentilä, Lassi; Zhang, Fengchun; Kyösti, Pekka; Pedersen, Gert F.

# Virtual Drive Testing of Adaptive Antenna Systems in Dynamic Propagation Scenarios for Vehicle Communications

Wei Fan, Lassi Hentilä, Fengchun Zhang, Pekka Kyösti, Gert F. Pedersen

*Abstract*—**Virtual drive testing (VDT) has gained great interest from both industry and academia, owing to its promise to replay field trials in a controllable laboratory condition. VDT is especially appealing for vehicle communication scenarios, where actual field trials can be difficult to carry out in practice. Research work on VDT of adaptive antenna systems in dynamic propagation scenarios has been limited, mainly due to high VDT setup cost and lack of efficient dynamic propagation channel models. In this paper, we propose to jointly emulate adaptive antennas (i.e. beamformers) and radio channels in the radio channel emulator to reduce the VDT setup cost. A simple dynamic propagation channel framework, which is based on linear interpolation of propagation parameters of the stationary channel models, is also presented. We further experimentally evaluate the beamformer capability (i.e. beam tracking and null steering) in dynamic line-of-sight (LOS) and non-LOS (NLOS) scenarios in the proposed cost-effective conducted VDT setups. The simulation and measurement results have demonstrated the effectiveness of the beam tracking and nulling steering algorithms in dynamic propagation conditions in the presence of interfering signal. The proposed setup and dynamic channel modeling framework are valuable for the VDT of adaptive antenna systems.**

## I. INTRODUCTION

To improve driving safety, vehicular sensors, e.g. ultrasonic sonars, cameras, laser scanners and radars, have been so far deployed on vehicles to detect obstacles in visual line-of-sight (LOS) scenarios and to avoid collisions [1], [2]. Wireless connectivity is seen as next major automotive innovation to provide infotainment service, to deliver a safe and autonomous driving experience in near future [3]. For example, it can make the detection of objects both in LOS and non-LOS (NLOS) conditions possible, to further improve driving safety [1], [4]. Long-term-evolution-vehicle (LTE-V) is envisioned as a key technology for intelligent transportation systems (ITS) due to its low cost and possibility of rapid deployment [5], [6].

Multiple-input multiple-output (MIMO) technique is seen as an enabling technology to offer high data-rate and reliable communications (both in LOS and NLOS scenarios) in next generation advanced driver assist systems. Unlike mobile terminals, the number of antennas in automotive application can be large, due to the large form factor. Automotive antennas

have been deployed for various radio applications. Further, adaptive antenna array technologies are seen vital in vehicular scenarios, where radio communications can be critical due to highly dynamic propagation channels and pervasive interfering signals.

Performance evaluation of antenna systems under realistic use scenarios is an essential step in product design and development. The antenna systems can be evaluated in the real network, so-called field trials. Field trials are mandatory to evaluate final system designs. In many cases field trials are uncontrollable and unrepeatable, due to weather and network conditions. If the system fails in field trials, it will be hard to identify design deficiencies in the development phase. In vehicle communications, field trials are even more challenging due to high mobility scenarios and more dynamic network conditions [7]–[10]. It would be desirable if the testing can be performed under repeatable laboratory conditions in early development cycle, where designers can quickly validate their performance and make rapid modifications to hardware and software designs. Moreover, it would be less expensive and less complicated to rectify issues in the early stage of development cycle.

Virtual drive test (VDT) has recently attracted great interest both from industry and academia [11]–[15]. The objective of VDT is to recreate an accurate real world representation of communication conditions in a controlled laboratory environment. In the VDT setup, real base stations (BSs) (or BS emulators) and user equipment (UE) are deployed, and radio channels, either recorded/simulated along the drive routes during a drive test or standard channel models, are implemented in the radio channel emulators (CEs). Both conducted cable setup and over-the-air (OTA) radiated setup have been discussed in the literature for system performance testing. VDT is appealing, since the testing can be done in an automated, controllable and repeatable manner, which can considerably reduce testing time and costs, and meanwhile accelerate actual infrastructure deployment. In commercial VDT toolsets, some propagation parameters and network conditions are recorded in the field testing. To perform VDT, missing propagation parameters are typically complemented with stochastic channel models [11], [12], [15]. In [13], the VDT setup implementing 3D ray tracing (RT) simulated channels is proposed and compared with actual field trials for a MIMO LTE vehicle to infrastructure (V2I) urban scenario. The VDT was performed in the conducted cable setup and it was proved to be a cost-effective alternative to expensive on-road field trials. [16] proposed a scheme to bring

Wei Fan, Fengchun Zhang, and Gert F. Pedersen are with the Antennas, Propagation and Millimeter-wave Systems section at the Department of Electronic Systems, Aalborg University, Denmark (email: {wfa}@es.aau.dk).
Lassi Hentilä is with Keysight, Finland.
P. Kyösti is with Keysight Technologies Finland Oy, Oulu, Finland (email: pekka.kyosti@keysight.com) and Centre for Wireless Communications (CWC), University of Oulu, Oulu, FI-90014 Finland.

measured site-specific propagation channels of a live LTE network to a VDT setup in a multi-probe anechoic chamber (MPAC) emulation environment for MIMO device testing. [17] and [18] proposed to reconstruct measured or RT simulated channels in the MPAC setup. [19]–[21] discussed a wireless cable method for OTA testing of antenna systems. The wireless cable method is especially attractive for large object equipped with a few non-adaptive antennas, e.g. automobile systems, since its setup cost is irrelevant to the test object size and channel models [20]–[22]. A framework to emulate random LOS propagation environment in the anechoic chamber was proposed for OTA testing of vehicular applications [23]. VDT testing of antenna systems on automobiles in the MPAC setup has attracted great attention in recent years, see e.g. in [1], [4]. VDT is a powerful and reliable tool when actual drive testing is difficult. However, the current research work reported in the literature on the VDT has been limited in several aspects:

1) Non-adaptive antenna systems equipped with few antennas have been targeted, e.g. LTE terminals. As discussed, for future wireless communication systems, the number of antennas can be high and antenna systems can be adaptive. As discussed in Section II, the existing VDT setups are cost-prohibitive for large-scale antenna systems. There is a strong need for suitable and cost-effective test setups for adaptive antenna systems.
2) Geometry-based stochastic channel (GBSC) models are often considered in VDT, since they are well-accepted in the industry and standardization. However, GBSC models fail to model realistic dynamic propagation scenarios, which are essential to evaluate adaptive antenna systems, e.g. the beam tracking and null steering capabilities. GBSCs are not site-specific and they are assumed stationary within a single drop (i.e. a snapshot of fading channels). GBSC models do not well support for spatial consistency. Deterministic channel models (e.g. RT simulated channels or recorded channels in the field), which characterize physical propagation parameters in a deterministic manner, are desirable. However, channel sounding is expensive and time-consuming, while ray-tracing simulation accuracy often suffers from inaccurate database description and high computation complexity. Deterministic channels are especially difficult to obtain in vehicle communication scenarios, since it would require high sampling rate in measurements in the high mobility scenario. There is a need for simple non-stationary GBSC models, which would allow performance evaluation of adaptive antenna systems.
3) Focus of VDT has been on performance evaluation of device under test (DUT) under desired radio channels, while interfering signals are often ignored in the VDT. As cell size is expected to get smaller for future wireless communication systems, co-channel interference (e.g. a user equipment (UE) receiving from other base station (BS)'s than the serving BS one) will become more significant and pervasive. Interference modeling has been considered in some commerical VDT tools, e.g. in [11]. The co-channel interference is signal of the same or
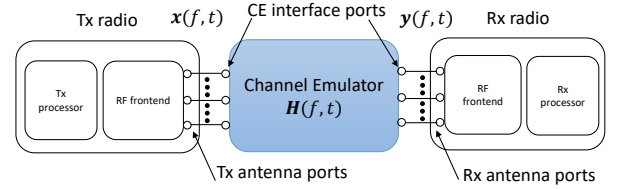


Figure 1. A schematic of the conducted setup.

similar type as the desired signal, and often will have the same type of propagation conditions. There is still a lack of research work on how adaptive antenna systems would operate in interfering signal conditions in the VDT setup.

In this paper, we first propose a cost-effective setup for VDT of adaptive antenna systems, as detailed in Section II. After that, we discuss a dynamic channel modeling framework in Section III, which is based on GBSC principle and easy to implement. Different beamformer algorithms of the adaptive antenna system are investigated in the dynamic LOS and NLOS channel conditions in Section IV and experimentally validated in Section V. Section VI concludes the paper and discusses future work directions.

## II. PROBLEM STATEMENT AND PROPOSED TESTING METHODOLOGY

As discussed in the introduction, two different testing setups have been discussed for the VDT, namely conducted cable testing and OTA radiated testing, as detailed below.

### A. Conducted Cable Testing

Antenna systems are typically equipped with accessible antenna connectors for conducted testing, where radio frequency (RF) testing signals can be guided to the DUT antenna ports using RF cables, bypassing the antennas. Therefore, the antenna characteristics are not considered in the conducted testing. This method is seen adequate when antenna performance is well known and the antenna count is small. A schematic of conducted setup is shown in Fig. 1. Neglecting the noise at the DUT antenna ports, the signal model can be written as:

$$\boldsymbol{y}(f,t) = \boldsymbol{H}(f,t)\boldsymbol{x}(f,t) \qquad (1)$$

where $\boldsymbol{x}(f,t)$ and $\boldsymbol{y}(f,t)$ denote the signal vector at the transmit antenna ports and DUT antenna ports, respectively. $\boldsymbol{H}(f,t)$ denotes the time-variant channel frequency transfer matrix between the transmit and receive antenna ports.

As can be seen, the CE interface ports are directly proportional to the number of antennas in the DUT. Conducted cable setup has been dominantly used in the industry for antenna system performance testing, mainly due to its simplicity and the small antenna count of antenna systems. However, the situation is rapidly changing for upcoming adaptive antenna systems, where antenna count can be large and antenna system will be adaptive. Antenna systems equipped with many

antennas would require many cable connections and associated RF hardware, leading to costly test setups. In the digital beamforming structure, where each DUT antenna is connected to the RF chain and antenna port, the DUT beamforming algorithms and operations can be tested, although the physical antenna elements and RF calibration impairments can not be considered. The conducted setup is not suitable for analog and hybrid beamforming structure.In hybrid or fully analog beamforming structures, each antenna port is associated with an antenna array (or sub-array).

### B. OTA Radiated Testing

OTA testing method is attractive, since it avoids RF cable connections to the DUT. That is, the DUT can be evaluated untouched, without the need to break the DUT case (e.g. automotive system). OTA radiated testing methods can be roughly grouped into two categories, namely the wireless cable method and environment emulation method, as discussed below:

- The wireless cable method is essentially an RF cable replacement technique, where one can achieve cable connection functionality, without actual RF cable connections [19]–[21]. The basic idea is that the transfer matrix between the OTA antenna ports and DUT antenna ports can be measured, and its (pseudo) inverse is then multiplied by the target channel models in the CE so that the desired signals are received at the respective DUT antenna ports. With this concept, the number of OTA antennas must be no less than the number of receive antennas on the DUT in principle. One has to calibrate out the transfer matrix, implying that the DUT antenna patterns must be static. As a summary, though highly attractive to replace cable test setup, the wireless cable method might not be suitable for adaptive antenna systems or antenna systems with a large antenna count. As illustrated in Fig. 2(a), the signal model for the wireless cable method can be written as:

$$\boldsymbol{y}(f,t) = \boldsymbol{A}\boldsymbol{A}^{-1}\boldsymbol{H}(f,t)\boldsymbol{x}(f,t) = \boldsymbol{H}(f,t)\boldsymbol{x}(f,t) \quad (2)$$

where $\boldsymbol{A}$ denotes the transfer matrix between the OTA antenna ports and DUT antenna ports. $()^{-1}$ denotes the (pseudo) inverse operator.

- The objective of environment emulation method is to characterize the complete end-to-end performance of wireless devices, via physically reproducing RF multipath environments in laboratory conditions [1], [16]–[18]. As illustrated in Fig. 2(b), the signal model for the environment emulation methods can be written in a general form as:

$$\boldsymbol{y}(f,t) = \boldsymbol{A}\boldsymbol{H}_{OTA}(f,t)\boldsymbol{x}(f,t) = \hat{\boldsymbol{H}}(f,t)\boldsymbol{x}(f,t) \quad (3)$$

where $\boldsymbol{A}$ is the transfer matrix between the OTA antenna ports and DUT antenna ports, and it is typically unknown. The goal of the channel emulation is to design channel matrix in the CE $\boldsymbol{H}_{OTA}(f,t)$ such that $\hat{\boldsymbol{H}}(f,t)$ approximates $\boldsymbol{H}(f,t)$. Note that spatial profiles of the channel models are required and they are physically mimicked, unlike the wireless cable method. OTA radiated methods
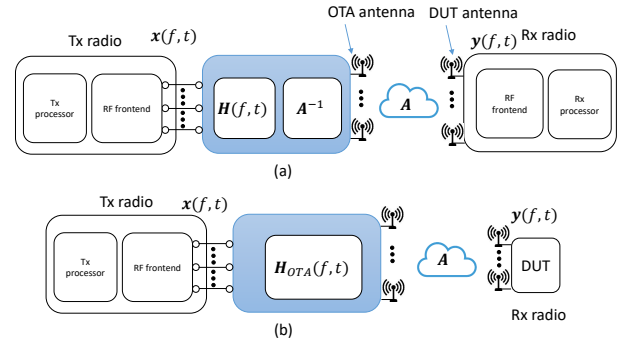


Figure 2. A schematic of OTA radiated setups. Figure (a) and (b) illustrate the wireless cable setup and environment emulation setup, respectively.

reported in the literature, either the multi-probe anechoic chamber (MPAC) method that offers a full control of emulated fields or the mode-stirrer reverberation chamber (RC) method which has a limited channel emulation flexibility, have been intensively discussed in industry and academia. It is commonly understood that RC might be less suitable for OTA testing of adaptive antenna systems since it does not offer control over angular distribution and polarization of the channel. The MPAC setup, though technically sound for OTA testing of adaptive antenna systems and allows true end-to-end performance testing, is expensive (i.e. it requires a high number of OTA antennas). This is especially the case when the DUT is electrically large or when we need three dimensional (3D) radio channel emulation in the MPAC setups.

### C. Proposed Cost-effective Testing Setup

To reduce the setup cost, we need to minimize the required CE interface ports and logical channels inside the CE. In the CE, input RF signals can be down-converted to baseband, digitized, convolved with radio channels at the baseband, converted to analog signal, and then up-converted. The radio channel model is typically mathematically implemented with a digital finite impulse response (FIR). In typical applications, only radio channels are modelled in the FIR coefficients. In principle, any system component that can be mathematically modeled, can be included in the time-variant FIR coefficients as well. In adaptive antenna systems, multiple antennas and RF front-ends are typically utilized for directional transmission or reception of a signal.

As discussed, the test setup cost is high in the existing conducted and OTA radiated setups, mainly due to the fact that the number of required CE interface ports are directly proportional to number of Tx/Rx antennas. Therefore, the setup cost can be significantly reduced if the adaptive antenna arrays (beamfomers) can be emulated inside the CE, jointly with radio channels, as illustrated in Fig. 3. Inspired by this, the FIR coefficients modeled in the CE is

$$\hat{h}(f,t) = \boldsymbol{w}_r^H(t)\boldsymbol{H}(f,t)\boldsymbol{w}_t(t) \quad (4)$$

where the term $t$ in the beamformer $\boldsymbol{w}_r$ and $\boldsymbol{w}_t$ denote the dynamic behaviour of the beamformer. The transmit and
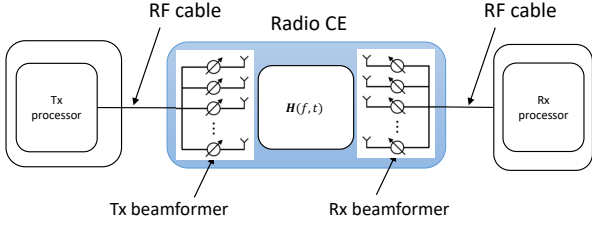
Figure 3. A schematic of the cost-effective setup.

receive beamforming weight vector can be obtained based on the directions of the target and interfering signals, and also the type of the beamformers. The direction of the signals can be determined via beam scanning procedures, e.g. the non beam-adaptive beam scanning procedure(i.e. no feedback required from the other end of radio node) discussed in [24] and adaptive beam scanning procedure in [25]. In this paper, we assume that the directions of the target and interfering signals are known based on the beam scanning algorithms.

The required number of CE interface ports only need to match the independent signal chains at the Tx and Rx side, not the actual number of Tx and Rx antennas as in the traditional conducted cable testing. This test setup can significantly reduce the setup cost for adaptive antenna systems, where multiple antennas and associated RF chains are utilized for one independent signal chain. The beamformer structure can be fully digital, fully analog, or hybrid, as long as the beamformer can be characterized by the beamforming weight vectors. The antenna pattern of each array element can be embedded in the radio channel model $\boldsymbol{H}$. Note that in the spatial multiplexing mode for LTE systems, the proposed setup might not help reduce the setup cost, since the number of independent signals are equivalent to the number of antennas. It is noted that though this joint emulation of Tx/Rx beamformers and the radio channel has the potential to the save hardware cost and complexity of the CE, it is not suitable for true end-to-end performance testing. Tx/Rx beamformers are typically inherent in the Tx/Rx radios and can not separately modeled as it is done in Fig. 3. However, it is still valuable in early development stage, e.g. for chip-set design, development and validation.

## III. Dynamic Channel Modeling and Adaptive Antenna Algorithms

In this section, we firstly describe the dynamic channel modelling framework proposed in [26]. After that, we describe the beamformer algorithms adopted in this paper. For the dynamic channel modeling part, the main contribution is that a complete framework for cost-effective dynamic channel model is derived.

### A. Dynamic Channel Modeling

*1) Stationary GBSC:* For a MIMO system equipped with $U$ antenna elements on the Rx side and $S$ antenna elements on the Tx side, the time-variant channel impulse response (CIR) $h_{u,s,n}(t,\tau)$ of the $n$th cluster with $n \in [1, N]$ between the $s$th

Tx antenna port and the $u$th Rx antenna port can be written as [26]–[29],

$$h_{u,s,n}(\tau,t) = \sqrt{\frac{K}{K+1}} h_{u,s}^{\text{los}}(\tau,t) + \sqrt{\frac{1}{K+1}} h_{u,s,n}^{\text{nlos}}(\tau,t), \quad (5)$$

where $K$ is the Rician K-factor. $h_{u,s}^{\text{los}}(\tau,t)$ and $h_{u,s,n}^{\text{nlos}}(\tau,t)$ denote the CIR for the LOS and NLOS part, respectively.

The CIRs for the LOS path can be further expressed as:

$$h_{u,s}^{\text{los}}(\tau,t) = \left[ \begin{array}{c} F_u^V(\Omega_{\text{los}}^{\text{Rx}}) \\ F_u^H(\Omega_{\text{los}}^{\text{Rx}}) \end{array} \right]^T \cdot \left[ \begin{array}{cc} \exp(j\Phi_{\text{los}}^{VV}) & 0 \\ 0 & \exp(j\Phi_{\text{los}}^{VV}) \end{array} \right],$$
$$\cdot \left[ \begin{array}{c} F_s^V(\Omega_{\text{los}}^{\text{Tx}}) \\ F_s^H(\Omega_{\text{los}}^{\text{Tx}}) \end{array} \right] \exp(j2\pi\vartheta_{\text{los}}t) \cdot \delta(\tau - \tau_{\text{los}}) \quad (6)$$

where $F_u^V$ and $F_u^H$ are the vertically polarized and horizontally polarized field pattern of the $u$th antenna element at the Rx, respectively. $F_s^V$ and $F_s^H$ are the vertically and horizontally polarized field pattern of the $s$th antenna element at the Tx, respectively. Note that the antenna field patterns are defined with a common phase center over the antenna array. $\Omega_{\text{los}}^{\text{Rx}}$, $\Omega_{\text{los}}^{\text{Tx}}$, $\vartheta_{\text{los}}$, $\tau_{\text{los}}$ denote the angle of departure, angle of arrival, Doppler frequency and delay of the LOS path, respectively. $\Phi_{\text{los}}^{VV}$ is the random initial phase for the LOS component.

The CIRs for the NLOS path can be further expressed as:

$$h_{u,s,n}^{\text{nlos}}(\tau,t) = \sqrt{\frac{p_n}{M}} \sum_m \left[ \begin{array}{c} F_u^V(\Omega_{n,m}^{\text{Rx}}) \\ F_u^H(\Omega_{n,m}^{\text{Rx}}) \end{array} \right]^T \cdot \boldsymbol{A}$$
$$\cdot \left[ \begin{array}{c} F_s^V(\Omega_{n,m}^{\text{Tx}}) \\ F_s^H(\Omega_{n,m}^{\text{Tx}}) \end{array} \right] \exp(j2\pi\vartheta_{n,m}t) \cdot \delta(\tau - \tau_n) \quad (7)$$

where $p_n$ and $\tau_n$ denote the power and delay of the $n$-th path, respectively. $\Omega_{n,m}^{\text{Rx}}$, $\Omega_{n,m}^{\text{Tx}}$, $\vartheta_{n,m}$ are the angle of arrival, angle of departure and Doppler frequency of the $m$-th sub-path in the $n$-th path with $m \in [1, M]$. $\boldsymbol{A}$ is the polarization matrix defined as:

$$\boldsymbol{A} = \left[ \begin{array}{cc} \exp(j\Phi_{n,m}^{VV}) & \sqrt{(\kappa_{n,m}^V)^{-1}}\exp(j\Phi_{n,m}^{VH}) \\ \sqrt{(\kappa_{n,m}^H)^{-1}}\exp(j\Phi_{n,m}^{HV}) & \exp(j\Phi_{n,m}^{HH}) \end{array} \right] \quad (8)$$

$\Phi_{n,m}^{VV}$, $\Phi_{n,m}^{VH}$, $\Phi_{n,m}^{HV}$ and $\Phi_{n,m}^{HH}$ are phase terms for the $m$th subpath in the $n$th path for four different polarization combinations, which are random variables following the uniform distribution in $[-180^o, 180^o]$. $\kappa_{n,m}^V$ and $\kappa_{n,m}^H$ are cross polarization ratios for the vertical and horizontal polarization.

As can be seen in (6) and (7), the time-variance of the CIR is generated by channel fading, while the propagation parameters are time-invariant.

*2) Non-stationary GBSC:* The non-stationary CIR for the LOS path can be generated as:

$$h_{u,s}^{\text{los}}(\tau,t) = \left[ \begin{array}{c} F_u^V(\Omega_{\text{los}}^{\text{Rx}}(t)) \\ F_u^H(\Omega_{\text{los}}^{\text{Rx}}(t)) \end{array} \right]^T \cdot \left[ \begin{array}{cc} \exp(j\Phi_{\text{los}}^{VV}) & 0 \\ 0 & \exp(j\Phi_{\text{los}}^{VV}) \end{array} \right],$$
$$\cdot \left[ \begin{array}{c} F_s^V(\Omega_{\text{los}}^{\text{Tx}}(t)) \\ F_s^H(\Omega_{\text{los}}^{\text{Tx}}(t)) \end{array} \right] \exp(j2\pi\vartheta_{\text{los}}(t) \cdot t) \cdot \delta(\tau - \tau_{\text{los}}(t)),$$
$$(9)$$

where time-variant LOS parameters $\Omega_{\text{los}}^{\text{Rx}}$, $\Omega_{\text{los}}^{\text{Tx}}$, $\vartheta_{\text{los}}$, $\tau_{\text{los}}$ can be dynamically calculated following the geometry of the Tx and Rx trajectories.

For the NLOS path, we have:

$$h_{u,s}^{\text{nlos}}(\tau,t) = \sqrt{\frac{p_n(t)}{M}} \sum_m \begin{bmatrix} F_u^V(\Omega_{n,m}^{\text{Rx}}(t)) \\ F_u^H(\Omega_{n,m}^{\text{Rx}}(t)) \end{bmatrix}^T \cdot \boldsymbol{A}(t)$$
$$\cdot \begin{bmatrix} F_s^V(\Omega_{n,m}^{\text{Tx}}(t)) \\ F_s^H(\Omega_{n,m}^{\text{Tx}}(t)) \end{bmatrix} \exp(j2\pi\vartheta_{n,m}(t) \cdot t) \cdot \delta(\tau - \tau_n(t))$$

(10)

where propagation parameters of each cluster for the NLOS path, including number of clusters, cluster delay, cluster power, cluster angle at the Tx and Rx side, cross-polarization power ratios (i.e. $\kappa_{n,m}^V$ and $\kappa_{n,m}^H$), can be made time-variant via linearly interpolating propagation parameter values of each cluster between two location snapshots. Note that in $\boldsymbol{A}(t)$, only terms $\kappa_{n,m}^V$ and $\kappa_{n,m}^H$ are time-variant, while the phase term are not time-variant. The number of clusters during the driving route might be varying. To achieve this, locations with lower number of clusters can be filled by clusters with insignificant power values, e.g. –100 dB [26]. It is noted that the Rician K-factor can be made time-variant via linearly interpolating K-factor values between two location snapshots.

The presented dynamic channel models allow dynamic evolution of the cluster parameters in spatial, temporal and polarimetric domains between specified location snapshots. It is attractive, since it is based on the well-accepted GBSC principles. Further, it is simple and easy to implement, since only linear interpolation of propagation parameters is needed.

### B. Beamformer Design

*1) Maximal ratio combining (MRC) beamformer:* The objective of the MRC BF is to combine antenna elements to improve signal strength in desired target signal directions. For a synthetic array, where gain patterns of all antenna elements are identical and phase patterns for all antenna elements can be calculated from the array structure, the $u$-th entry of $\boldsymbol{w}(\theta,\phi)$ is given by [30], [31]

$$w^u(\theta,\phi) = \frac{1}{U} \exp(-j\langle \boldsymbol{k}(\theta,\phi), \boldsymbol{r}_u \rangle),$$
$$\boldsymbol{k}(\theta,\phi) = \frac{2\pi f}{c} (\cos\theta\cos\phi, \cos\theta\sin\phi, \sin\theta),$$
$$\boldsymbol{r}_u = (x_u, y_u, z_u),$$

(11)

where $\boldsymbol{k}(\theta,\phi)$ is the wave vector with $c$ denoting the speed of light. $\boldsymbol{r}_u$ is the location vector of the $u$-th Rx antenna, and $\langle \boldsymbol{v}_1, \boldsymbol{v}_2 \rangle$ returns the inner product of vector $\boldsymbol{v}_1$ and $\boldsymbol{v}_2$. $\theta$ and $\phi$ denote the elevation and azimuth angle of the path, respectively. For real antenna arrays, the gain patterns of the elements, though similar, are different due to mutual coupling, edge effect and practical designs. The phase patterns are embedded in the measured radiation patterns. The beamformer can be obtained directly from the measured complex antenna patterns, as discussed in [31].

The MRC weight vector to steer the beam towards target signal direction $(\theta_s, \phi_s)$ is therefore:

$$\boldsymbol{w}_{MRC} = \boldsymbol{w}(\theta_s, \phi_s)$$

(12)

*2) Zero forcing (ZF) beamformer:* The objective is to form the beam to the target signal direction and the null to the interfering signal direction, and this can be achieved using the ZF beamformer. As discussed in [32], the weight vector $\boldsymbol{w}$ can be given as

$$\boldsymbol{w}_{ZF} = \boldsymbol{w}_{MRC}(\boldsymbol{I}_U - \boldsymbol{P}_c),$$

(13)

where $\boldsymbol{w}_{MRC}$ is defined in (11) to form the beam to the target signal direction $\theta_s$ and $\phi_s$. $\boldsymbol{I}_U$ is a $U \times U$ identity matrix, and the matrix $\boldsymbol{P}_c \in \boldsymbol{C}^{U \times U}$ is to place the nulls to the interfering signal direction. $\boldsymbol{P}_c$ can be expressed as

$$\boldsymbol{P}_c = \boldsymbol{w}(\theta_i, \phi_i)[\boldsymbol{w}^H(\theta_i, \phi_i)\boldsymbol{w}(\theta_i, \phi_i)]^{-1}\boldsymbol{w}^H(\theta_i, \phi_i),$$

(14)

where $()^H$ denotes Hermitian transpose operator and $\boldsymbol{w}_i^H(\theta_i, \phi_i)$ is obtained in (11). Note that (14) can be extended to the case where multiple interfering signals exist.

### IV. SIMULATION RESULTS

In the simulations, both the LOS and NLOS scenarios are considered, as illustrated in Fig. 4 and Fig. 7, respectively. Two BSs, one functioning as the serving BS (BS1) and one as the interfering BS (BS2), are utilized. Each BS antenna is equipped with a vertically polarized dipole antenna. At the mobile station (MS) side, a uniform circular array (UCA), which is equipped with eight vertically polarized dipole antennas (with half wavelength spacing), is assumed. In the simulations, vertically polarized dipole antennas and 2D propagation channels (i.e. propagation paths only on the azimuth plane), are assumed for the sake of simplicity. It is noted that the dynamic channel modeling supports for arbitrary antenna patterns at the Tx and Rx side, and 3D propagation channels, as explained in Section III-A. In the simulation, only the receive beamformer is considered as an example. The speed of travel is set to 30 km/h as an example. In the simulation, it is assumed that the beamformer can support real-time beam forming and null steering operations.

### A. LOS Scenario

In the LOS scenario, a pure specular LOS path is considered between each BS and the MS location for the sake of simplicity. As discussed, the dynamic evolution of the LOS path parameters, including power, angle of departure, angle of arrival, delay and Doppler frequency can be determined from the BS and MS geometry, as shown in Fig. 4. The time-varying angles of arrival of the LOS paths corresponding to BS1 and BS2 are shown in Fig. 5, which are denoted in black and red curves, respectively in the figure. The dynamic MRC and ZF beamformer pattern are shown in Fig. 5 (left) and Fig. 5 (right), respectively. It can be clearly observed that with the MRC beamformer the array main beam is always steered towards to the LOS path from the serving cell (i.e. the black curve). As for the ZF beamformer, the beam is always steered towards to the LOS path from the serving cell (i.e. the black curve), while the null is steered to the LOS path from the interfering cell at the same time (i.e. the red curve), as expected. The beam
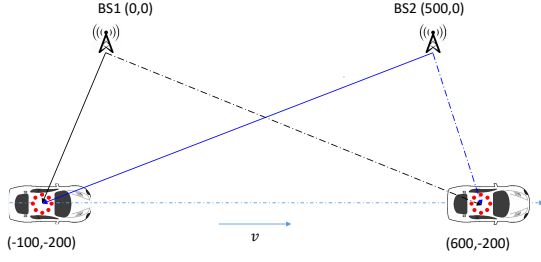
Figure 4. An illustration of the LOS scenario. The coordinates of the BSs and starting and end location of the MS are shown.
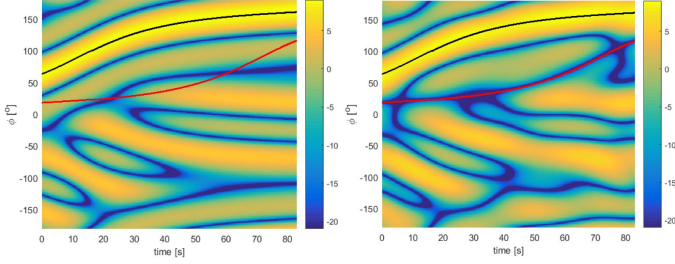


Figure 5. Time-variant array pattern using MRC (left) and ZF (right) beamformers in the LOS scenario.
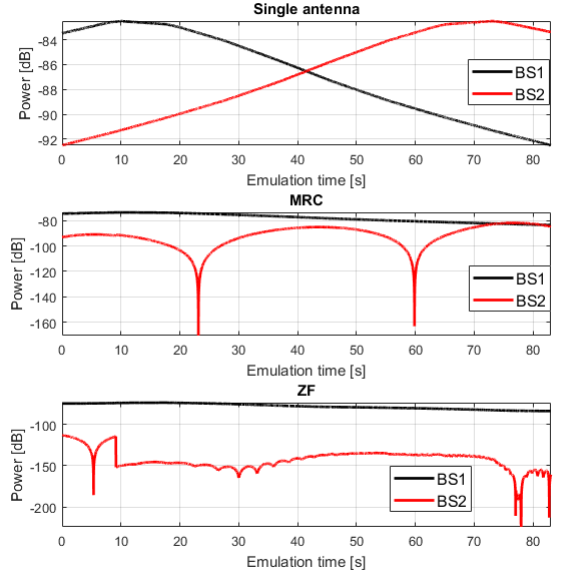


Figure 6. Channel gain for single angle (top), UCA with MRC beamformer (middle) and UCA with ZF beamformer (bottom) for BS1 and BS2 in the LOS scenario. Note that the power range are set differently in the plots.
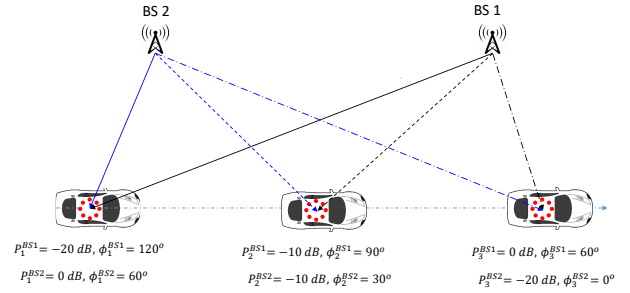


Figure 7. An illustration of the NLOS scenario.

tracking and null steering operation of the adaptive array in dynamic LOS channel conditions can be clearly observed.

The channel gains (i.e. $20\log_{10}|\hat{h}_{11}(t)|$ for BS1 and $20\log_{10}|\hat{h}_{12}(t)|$ for BS2) of the MRC and ZF beamformer in the dynamic LOS scenario are shown in Fig. 6. As a reference, channel gain of a single antenna at the MS side is shown as well in the figure (top). The power of the LOS path corresponding to BS1 and BS2 can be observed in Fig. 6 (top). The power value of the LOS path from BS1 increases while the vehicle is moving closer to the BS, and it decreases as the vehicle is moving away, as can be seen in Fig. 4. This can also be observed for the LOS path from BS2. The signal to interference ratio (SIR), which is the key performance indicator, will continue to decrease as the MS is moving from BS1 towards BS2. As for the MRC beamformer, a gain of around 9 dB (i.e. $10\log_{10}(8)$) for the target LOS path compared to the single antenna case is achieved along the whole driving route, as expected (black curve). The interfering LOS path is spatially filtered by the sidelobe of dynamic MRC beamformer array pattern, as shown in Fig. 5. The SIR level is low when the MS is close to BS2, as can be seen in Fig. 6. For the ZF beamformer, a gain of around 9 dB for the target LOS path compared to the single antenna case is also observed, as expected. The channel gain for the interfering LOS path is significantly reduced, due to the fact the null is always steered towards to the dynamic interfering LOS path, as shown in Fig. 5. An excellent SIR level can be therefore guaranteed along the route for the ZF beamformer.

### B. NLOS scenario

In the NLOS scenario, a single spatial cluster with a truncated Laplacian shape is considered for each BS for the sake of simplicity. In the simulation, three MS locations are specified, as illustrated in Fig. 7. For each MS location, we can set the cluster parameters. For the two clusters (one for BS1 and the other for BS2), the cluster parameters, angle spread of arrival, angle of departure, angle spread of departure and delay for fixed and set to $10^o$, $0^o$, $10^o$, 0ns respectively. The power value and angle of arrival of the two clusters for the three locations specified in Fig. 7. The cluster parameters between two MS locations and linearly interpolated, as explained in Section III-A. The time-varying angles of arrival of the cluster corresponding to BS1 and BS2 are shown in Fig. 8, which are denoted in black and red curves, respectively in the figure. It is noted that the cluster parameters are not determined from the geometry for the NLOS scenario.

The MRC and ZF beamformer array pattern are shown in Fig. 8 (left) and Fig. 8 (right), respectively. Similar to the LOS scenario, the beam tracking and null steering operation of the adaptive array in dynamic NLOS channel conditions can be clearly observed. Note that the cluster mean angle of arrivals are utilized as the direction of the cluster in the simulation for BF designs.

The channel gains in the dynamic NLOS scenario for different antenna and beamformer configurations are shown in
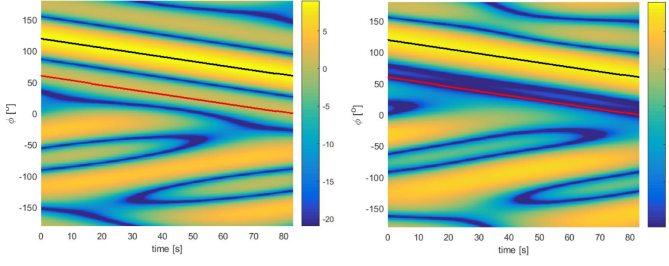
Figure 8. Time-variant array pattern using MRC (left) and ZF (right) beamformers in the NLOS scenario.
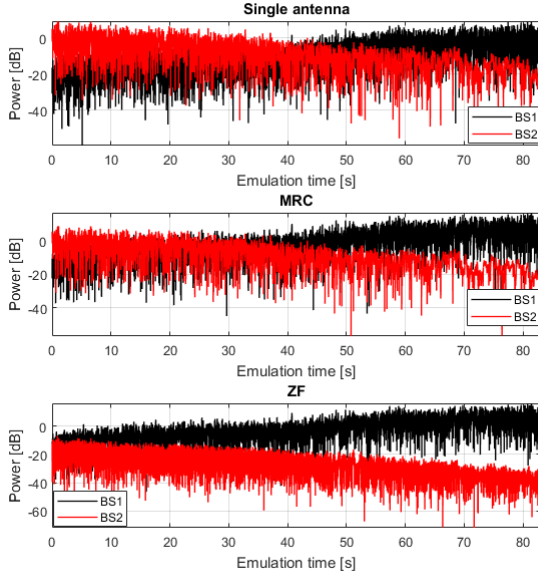


Figure 9. Channel gain for single angle (top), UCA with MRC beamformer (middle) and UCA with ZF beamformer (bottom) for BS1 and BS2 in the NLOS scenario.

Fig. 9. For the single antenna case, it can be clearly observed that average power for the serving cell is increasing, while the one for interfering cell is decresing. This is consistent with power settings specified in Fig. 7 (i.e. -20 dB to 0 dB for target path, and 0 dB to -20 dB for interfering path along the driving route). Similar to the LOS scenario, a gain of around 9 dB for the average power of target cluster can be achieved for the MRC beamformer, compared to the single antenna case. As for the ZF beamformer, a gain of around 9 dB for the target path and a significant reduction of the interfering path can be also observed, as expected.

## V. THROUGHPUT MEASUREMENT AND RESULT ANALYSIS

### A. Measurement Setup

The VDT measurement setup is illustrated in Fig. 10. A photo of the practical setup can be found in [33]. A BS emulator and an LTE phone were utilized to mimic the serving cell (BS1) and the LTE receiver. A radio CE was utilized for two purposes: 1) the interfering LTE BS (BS2) behavior and setting can be internally mimicked in the CE; 2) the joint emulation of channel profiles and Rx beamformer can be implemented in the CE for BS1 and BS2, as illustrated
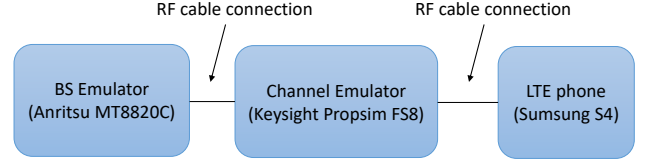


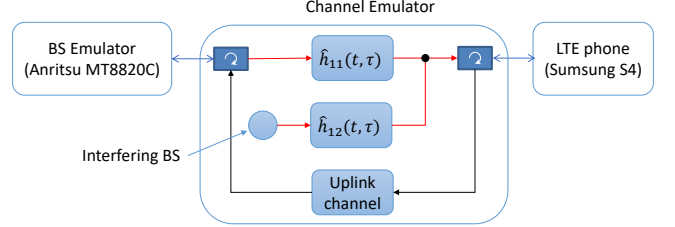Figure 10. An illustration of the measurement setup.



Figure 11. A schematic of communication link established in the setup. The downlink and uplink are denoted in red and black lines, respectively. The uplink channel was bypassed in the CE.

in Fig. 11. As shown in Fig. 11, only two bi-directional CE interface ports and three logical channels are utilized to enable the bi-directional communication in the CE. In the VDT setup, only one RF cable connection is utilized to guide the RF signal for the CE input and output ports. The VDT setup complexity and cost can be greatly reduced, compared to conventional conducted cable setup and OTA radiated setup. The dynamic channel models and dynamic Rx beamfomers (i.e. support of beam-tracking in the MRC and beam-tracking and null-steering in the ZF beamformer) are implemented in the channel profiles $\hat{h}_{11}(t,\tau)$ and $\hat{h}_{12}(t,\tau)$ for the BS1 and BS2, respectively. The detailed setting of each system component is shown in Table I. Note that the noise is not modeled in the measurement. A total of six throughput measurements were performed (i.e. three different MS beamforming topologies for two dynamic channel models). Note for easy exhibition, we use the throughput percent in the plots, defined as the throughput normalized by its maximum value (17.712 Mbit/s).

### B. Measurement Results

The measured throughput results in the dynamic LOS scenario are shown in Fig. 12. The measured throughput is determined by the SIR at the receiver. When the SIR level is high (i.e. SIR above a threshold), the measured throughput can reach the peak. When the SIR level is below the threshold, the measured throughput will abruptly drop to zero. It was explained in [34] that with modern forward error correction (FEC) codes, the change in terms of error rate is very abrupt, from almost 100% to almost 0% at a specific signal threshold level in the LOS conditions. As explained in Fig. 6, for a single element, the SIR will continue to drop along the driving route. In the measured throughput curve, the abrupt change occurs around 40s. For the MRC beamformer, the SIR is improved, as the signal level is boosted around 9 dB. As a result, the abrupt change occurs much later (at the end of route where interference is high). For the ZF beamformer,

## Table I
### Setup and specifications of each component in the measurement system

| Component | Setup and specifications |
|---|---|
| BS emulator | • Model: Anritsu MT8820C<br>• Frame structure: frequency division duplex (FDD)<br>• LTE frequency band: 3; Downlink frequency: 1842.5 MHz; Uplink frequency: 1747.5 MHz<br>• Channel bandwidth: 10 MHz<br>• Transmission mode: TM 1 (i.e. single transmit antenna) |
| Radio CE | • Model: Keysight Propsim FS 8<br>• Interfering BS: same settings as the BS1 in the BS emulator. It is noted that the transmission mode is fixed to TM2 (transmit diversity) in the Prosim CE setting. To ensure same transmission mode as the serving cell (BS1), one branch is disabled.<br>• Channel models: as shown in Fig. 11. Note $\hat{h}_{11}(t,\tau)$ and $\hat{h}_{12}(t,\tau)$ contain both the channel profiles and Rx beamformer. |
| MS | • Model: Samsung Galaxy S4. It is noted that only one antenna port was used and the other one was properly terminated. |
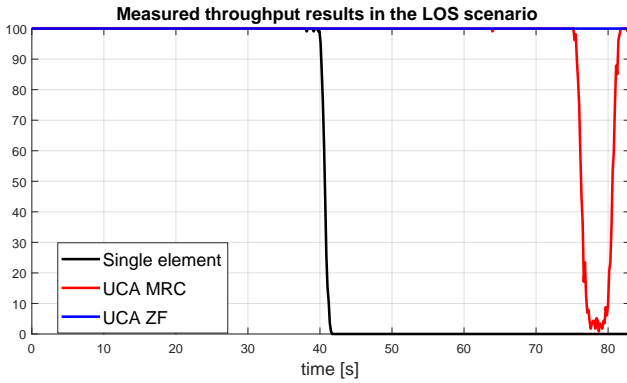


Figure 12. Measured throughput results for different Rx beamformer algorithms in the dynamic LOS scenario.

maximum throughput along the whole driving route can be achieved, due to the strong interference rejection introduced by the null steering (i.e. a high SNR is always guaranteed).

The measured throughput results in the dynamic NLOS scenario are shown in Fig. 13. At the beginning of the route, the interfering signal is strong, as explained in Fig. 9. The SIR level increases along the driving route for the NLOS scenario. The measured throughput results generally agree with the SIR observations. For the NLOS scenario, the measured throughput results strongly fluctuate due to the channel fading. Similar to the LOS scenario, throughput measured with the MRC beamformer outperforms the one measured with single antenna due to the BF gain for the target signal. The throughput measured with the ZF beamformer clearly outperforms the MRC algorithm, since the interfering signal level is significantly reduced.
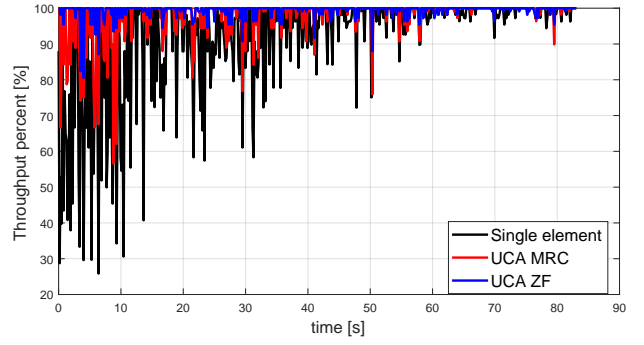


Figure 13. Measured throughput results for different Rx beamformer algorithms in the dynamic NLOS scenario.
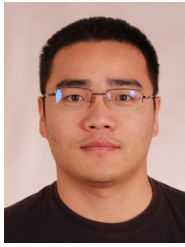
## VI. Conclusion

VDT is a powerful and cost-effective alternative to actual field trials to evaluate antenna system performance. For critical scenarios where propagation channels are highly dynamic and antenna systems are adaptive, VDT is even more appealing due to difficulties in field trials. In this paper, a joint emulation of beamformer at the Tx and Rx side and radio channel model in the CE is proposed. Compared to conventional conducted cable and radiated OTA VDT setups, the system cost and complexity is greatly reduced since fewer channel emulator interface ports and logical channels are needed. Further, a simple dynamic channel modeling framework based on GBSC principles and linear interpolation of stationary channel models is presented for evaluating adaptive antenna systems. Two beamformer designs are evaluated, namely the MRC scheme to boost target signal strength and ZF scheme to simultaneously boost target signal and reject undesired interference. We experimentally evaluate the two beamformer designs under dynamic LOS and NLOS conditions in the proposed VDT setup. The simulation and measurement results have demonstrated the effectiveness of the beam tracking and nulling steering algorithms in dynamic propagation conditions in the presence of interfering signal.

In this paper, a synthetic antenna array (i.e. UCA) with well-known beamforming algorithms (i.e.. MRC and ZF) is evaluated under simple LOS and NLOS dynamic channel models to demonstrate the proposed cost-effective VDT setup. The beamformer is designed, assuming known impinging angles of the target and interfering spatial profiles. There are a few logical extension of current work. Realistic antenna array (either measured in an anechoic chamber or simulated) can be used to replace the synthetic array. Different beamformer design criterion can be evaluated in the proposed framework, e.g. number of beams and beam-width at UE and BS side, beamformer update rate, etc. More realistic dynamic channel models can be considered as well.

to acknowledge the assistance from colleagues in Keysight Technologies in the practical measurement.



**Wei Fan** received his Bachelor of Engineering degree from Harbin Institute of technology, China in 2009, Master's double degree with highest honours from Politecnico di Torino, Italy and Grenoble Institute of Technology, France in 2011, and Ph.D. degree from Aalborg University, Denmark in 2014. From February 2011 to August 2011, he was with Intel Mobile Communications, Denmark as a research intern. He conducted a three-month internship at Anite telecoms oy, Finland in 2014. His main areas of research are over the air testing of multiple antenna systems, radio channel sounding, modeling and emulation. He is currently an associate professor at the Antennas, Propagation and Millimeter-wave Systems (APMS) Section at Aalborg University.



**Lassi Hentilä** received the M.Sc. degree in telecommunication from the University of Oulu, Finland in 2004. From 2004 to 2016, he was with Elektrobit/Anite. Since 2004, he has been involved in radio channel measurements, modeling and emulation. He was moved to Keysight Technologies Finland Oy along the acquisition in 2016. He is currently involved in channel modeling and testing methodology for 5G systems with Keysight Technologies Finland Oy.
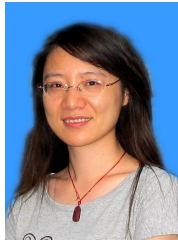


**Fengchun Zhang** received her B.Sc. degree in optical information science and technology, and the M. Sc. in acoustics from the South China University of Technology, Guangzhou, China, in 2006 and 2009, respectively. She is currently a Ph.D. fellow with the Department of Electronics Systems, Aalborg University, Aalborg, Denmark. Her research interests are in antenna array signal processing, beamforming, parameter estimation for channel characterization of centimeter and millimeter wave wireless systems.



**Pekka Kyösti** received the M.Sc. degree in mathematics from the University of Oulu, Finland. From 1998 to 2002, he was with Nokia Networks. From 2002 to 2016, he was with Elektrobit/Anite. Since 2002, he has been involved in radio channel measurements, estimation and modeling. From 2008 to 2012, he was actively developing methods for MIMO over-the-air testing. He was moved to Keysight Technologies Finland Oy along the acquisition in 2016. He is currently involved in channel modeling for 5G systems with Keysight Technologies Finland Oy and with the University of Oulu.



**Gert Frølund Pedersen** was born in 1965 and married to Henriette and have 7 children. He received the B.Sc. E. E. degree, with honour, in electrical engineering from College of Technology in Dublin, Ireland in 1991, and the M.Sc. E. E. degree and Ph. D. from Aalborg University in 1993 and 2003. He has been with Aalborg University since 1993 where he is a full Professor heading the Antenna, Propagation and Networking LAB with 36 researcher. Further he is also the head of the doctoral school on wireless communication with some 100 phd students enrolled. His research has focused on radio communication for mobile terminals especially small Antennas, Diversity systems, Propagation and Biological effects and he has published more than 175 peer reviewed papers and holds 28 patents. He has also worked as consultant for developments of more than 100 antennas for mobile terminals including the first internal antenna for mobile phones in 1994 with lowest SAR, first internal triple-band antenna in 1998 with low SAR and high TRP and TIS, and lately various multi antenna systems rated as the most efficient on the market. He has worked most of the time with joint university and industry projects and have received more than 12 M$ in direct research funding. Latest he is the project leader of the SAFE project with a total budget of 8 M$ investigating tunable front end including tunable antennas for the future multiband mobile phones. He has been one of the pioneers in establishing Over-The-Air (OTA) measurement systems. The measurement technique is now well established for mobile terminals with single antennas and he was chairing the various COST groups (swg2.2 of COST 259, 273, 2100 and now ICT1004) with liaison to 3GPP for over-the-air test of MIMO terminals. Presently he is deeply involved in MIMO OTA measurement.

## REFERENCES

[1] M. G. Nilsson, P. Hallbjörner, N. Arabäck, B. Bergqvist, T. Abbas, and F. Tufvesson, "Measurement uncertainty, channel simulation, and disturbance characterization of an over-the-air multiprobe setup for cars at 5.9 ghz," *IEEE Transactions on Industrial Electronics*, vol. 62, no. 12, pp. 7859–7869, 2015.

[2] B. Fleming, "An overview of advances in automotive electronics [automotive electronics]," *IEEE Vehicular Technology Magazine*, vol. 9, no. 1, pp. 4–9, March 2014.

[3] J. Harding, G. Powell, R. Yoon, J. Fikentscher, C. Doyle, D. Sade, M. Lukuc, J. Simons, and J. Wang, "Vehicle-to-vehicle communications: Readiness of v2v technology for application," Tech. Rep., 2014.

[4] M. Nilsson, P. Hallbjörner, N. Arabäck, B. Bergqvist, and F. Tufvesson, "Multipath propagation simulator for v2x communication tests on cars," in *Antennas and Propagation (EuCAP), 2013 7th European Conference on*. IEEE, 2013, pp. 1342–1346.

[5] D. W. Matolak, Q. Wu, J. J. Sanchez-Sanchez, D. Morales-Jiménez, and M. C. Aguayo-Torres, "Performance of lte in vehicle-to-vehicle channels," in *Vehicular Technology Conference (VTC Fall), 2011 IEEE*. IEEE, 2011, pp. 1–4.

[6] R. He, B. Ai, G. Wang, K. Guan, Z. Zhong, A. F. Molisch, C. Briso-Rodriguez, and C. P. Oestges, "High-speed railway communications: From gsm-r to lte-r," *IEEE Vehicular Technology Magazine*, vol. 11, no. 3, pp. 49–58, Sept 2016.

[7] K. Guan, B. Ai, A. Fricke, D. He, Z. Zhong, D. W. Matolak, and T. Kürner, "Excess propagation loss modeling of semiclosed obstacles for intelligent transportation system," *IEEE Transactions on Intelligent Transportation Systems*, vol. 17, no. 8, pp. 2171–2181, Aug 2016.

[8] K. Guan, B. Ai, M. L. Nicolas, R. Geise, A. Müller, Z. Zhong, and T. Kürner, "On the influence of scattering from traffic signs in vehicle-to-x communications," *IEEE Transactions on Vehicular Technology*, vol. 65, no. 8, pp. 5835–5849, Aug 2016.

[9] R. He, O. Renaudin, V. M. Kolmonen, K. Haneda, Z. Zhong, B. Ai, and C. Oestges, "Characterization of quasi-stationarity regions for vehicle-to-vehicle radio channels," *IEEE Transactions on Antennas and Propagation*, vol. 63, no. 5, pp. 2237–2251, May 2015.

[10] ——, "A dynamic wideband directional channel model for vehicle-to-vehicle communications," *IEEE Transactions on Industrial Electronics*, vol. 62, no. 12, pp. 7870–7882, Dec 2015.

[11] Anite, "Virtual drive testing toolset," February 2015. [Online]. Available: http://www.anite.com/virtualdrivetesting

[12] A. S. Erik Org, "Field-to-lab infuses the real world into mobile-device virtual testing," December 2011. [Online]. Available: http://mobiledevdesign.com/learning-resources/field-lab-infuses-real-world-mobile-device-virtual-testing-0

[13] M. Charitos, D. Kong, J. Cao, D. Berkovskyy, A. A. Goulianos, T. Mizutani, F. Tila, G. Hilton, A. Doufexi, and A. Nix, "Lte-a virtual drive testing for vehicular environments," in *VTC 2017, Spring*. IEEE, 2017.

[14] P. Kyösti, T. Jämsä, and J.-P. Nuutinen, "Channel modelling for multiprobe over-the-air MIMO testing," *International Journal of Antennas and Propagation*, vol. 2012, 2012.

[15] Spirent, "Spirent virtual drive test (VDT)-conversion tool," February 2015. [Online]. Available: http://www.spirent.com/Products/Virtual_Drive_Testing

[16] P. Kyösti, P. Kemppainen, and T. Jämsä, "Radio channel measurements in live lte networks for mimo over-the-air emulation," in *The 8th European Conference on Antennas and Propagation (EuCAP 2014)*, April 2014, pp. 3679–3683.

[17] J. T. Toivanen, T. A. Laitinen, V. M. Kolmonen, and P. Vainikainen, "Reproduction of arbitrary multipath environments in laboratory conditions," *IEEE Transactions on Instrumentation and Measurement*, vol. 60, no. 1, pp. 275–281, Jan 2011.

[18] W. Fan, I. Carton, P. Kyösti, and G. F. Pedersen, "Emulating ray-tracing channels in multiprobe anechoic chamber setups for virtual drive testing," *IEEE Transactions on Antennas and Propagation*, vol. 64, no. 2, pp. 730–739, 2016.

[19] C. Schirmer, M. Lorenz, A. T. Wim, R. Perthold, M. H. Landmann, G. Del Galdo *et al.*, "Mimo over-the-air testing for electrically large objects in non-anechoic environments," in *Antennas and Propagation (EuCAP), 2016 10th European Conference on*. IEEE, 2016, pp. 1–6.

[20] W. Yu, Y. Qi, K. Liu, Y. Xu, and J. Fan, "Radiated two-stage method for lte mimo user equipment performance evaluation," *IEEE Transactions on Electromagnetic Compatibility*, vol. 56, no. 6, pp. 1691–1696, Dec 2014.

[21] W. Fan, P. Kyösti, L. Hentilä, and G. F. Pedersen, "Mimo terminal performance evaluation with a novel wireless cable method," *IEEE Transactions on Antennas and Propagation*, vol. 65, no. 9, pp. 4803–4814, Sept 2017.

[22] M. D. Foegelle, "The future of mimo over-the-air testing," *IEEE Communications Magazine*, vol. 52, no. 9, pp. 134–142, September 2014.

[23] M. S. Kildal, A. A. Glazunov, J. Carlsson, and A. Majidzadeh, "Evaluation of a simplified random-los measurement setup for characterizing antennas on cars," in *Antennas and Propagation (EUCAP), 2017 11th European Conference on*. IEEE, 2017, pp. 3007–3011.

[24] D. Hui, J. Axnäs, and R. Baldemair, "Efficient beam scanning for high-frequency wireless networks," Nov. 3 2014, uS Patent App. 14/531,494.

[25] S. Hur, T. Kim, D. J. Love, J. V. Krogmeier, T. A. Thomas, and A. Ghosh, "Multilevel millimeter wave beamforming for wireless backhaul," in *2011 IEEE GLOBECOM Workshops (GC Wkshps)*, Dec 2011, pp. 253–257.

[26] L. Hentilä, P. Kyösti, and P. Heino, "Evaluation of beam forming and multi antenna techniques in non-stationary propagation scenarios with hw emulator," in *2012 International ITG Workshop on Smart Antennas (WSA)*, March 2012, pp. 347–351.

[27] "Spatial channel model for Multiple Input Multiple Output (MIMO) simulations," 3GPP, TR 25.996 V12.0.0, Sep. 2014.

[28] J. Meinilä, P. Kyösti, T. Jämsä, and L. Hentilä, "Winner ii channel models," *Radio Technologies and Concepts for IMT-Advanced*, pp. 39–92.

[29] L. Hentilä, P. Kyösti, and J. Meinilä, "Elevation extension for a geometry-based radio channel model and its influence on mimo antenna correlation and gain imbalance," in *Proceedings of the 5th European Conference on Antennas and Propagation (EUCAP)*, April 2011, pp. 2175–2179.

[30] C. A. Balanis, "Antenna theory: A review," *Proceedings of the IEEE*, vol. 80, no. 1, pp. 7–23, 1992.

[31] F. Zhang, W. Fan, J. Zhang, and G. F. Pedersen, "Virtual large-scale array beamforming analysis using measured subarray antenna patterns," *IEEE Access*, vol. 5, pp. 19 812–19 823, 2017.

[32] H. L. Van Trees, *Optimum array processing: Part IV of detection, estimation and modulation theory*. Wiley Online Library, 2002, vol. 1.

[33] W. Fan, P. Kyösti, Y. Ji, L. Hentilä, X. Chen, and G. F. Pedersen, "Experimental evaluation of user influence on test zone size in multiprobe anechoic chamber setups," *IEEE Access*, vol. 5, pp. 18 545–18 556, 2017.

[34] P.-S. Kildal, A. Hussain, X. Chen, C. Orlenius, A. Skarbratt, J. Asberg, T. Svensson, and T. Eriksson, "Threshold receiver model for throughput of wireless devices with mimo and frequency diversity measured in reverberation chamber," *IEEE Antennas and Wireless Propagation Letters*, vol. 10, pp. 1201–1204, 2011.